ADVANCED MATERIALS
www.advmat.de

A Mechanoresponsive Phase-Changing Electrolyte Enables Fabrication of High-Output Solid-State Photobioelectrochemical Devices from Pigment-Protein Multilayers

*Sai Kishore Ravi, David J. K. Swainsbury, Varun Kumar Singh, Yoke Keng Ngeow, Michael R. Jones, and Swee Ching Tan**

Exploitation of natural photovoltaic reaction center pigment proteins in biohybrid architectures for solar energy harvesting is attractive due to their global abundance, environmental compatibility, and near-unity quantum efficiencies. However, it is challenging to achieve high photocurrents in a device setup due to limitations imposed by low light absorbance by protein monolayers and/or slow long-range diffusion of liquid-phase charge carriers. In an attempt to enhance the photocurrent density achievable by pigment proteins, here, an alternative solid-state device architecture enabled by a mechanoresponsive gel electrolyte that can be applied under nondenaturing conditions is demonstrated. The phase-changing electrolyte gel provides a pervading biocompatible interface for charge conduction through highly absorbing protein multilayers that are fabricated in a simple fashion. Assembled devices exhibit enhanced current stability and a maximal photoresponse of ≈860 μA cm^{-2}, a fivefold improvement over the best previous comparable devices under standard illumination conditions. Photocurrent generation is enhanced by directional energy transfer through extended layers of light-harvesting complexes, mimicking the modular antenna/transducer architecture of natural photosystems, and by metastable radical pair formation when photovoltaic reaction centers are embedded throughout light-harvesting regions of the device.

As part of the development of more varied, sustainable, and ecofriendly light-harvesting technologies, there is growing interest in either mimicking or directly exploiting natural photosynthetic complexes.[1,2] In addition to inspiring the design of molecular systems for artificial photosynthesis,[3] photosynthetic pigment proteins have been directly interfaced with electrodes for potential applications in photobioelectrochemical cells, biosensing, photodetection, solar fuel synthesis, and biocomputing.[4–7] Much of this effort has focused on the reaction centre (RC) complex from purple photosynthetic bacteria[8] and the larger RC–LH1 complex that is assembled between this RC and the so-called LH1 light-harvesting protein[9] (see Figure S1 in the Supporting Information). This RC facilitates a multistep charge separation between a pair of bacteriochlorophylls (P) and a quinone electron acceptor (Q_B) with a very high quantum efficiency[8,10,11] (**Figure 1**a; Figure S1, Supporting Information). Photocurrents from these proteins have typically been studied in open, three-electrode cells incorporating a protein-coated working electrode immersed in a buffer containing a mobile, small molecule electrolyte.[12–22] Two-electrode sealed liquid cells with one or more mobile mediators have also been constructed.[23–25] Proteins are typically adhered to the working electrode by drop casting or adsorption from solution, although electrospraying[20] and laser-induced forward transfer[26] have also been explored. Photocurrents from such devices frequently show an initial spike of "peak current" that decays over seconds or minutes to

S. K. Ravi, Dr. V. K. Singh, Prof. S. C. Tan
Department of Materials Science and Engineering
National University of Singapore
9 Engineering Drive 1, Singapore 117575, Singapore
E-mail: msetansc@nus.edu.sg

The ORCID identification number(s) for the author(s) of this article can be found under https://doi.org/10.1002/adma.201704073.

[+]Present address: Department of Molecular Biology and Biotechnology, University of Sheffield, Sheffield S10 2TN, UK

Dr. D. J. K. Swainsbury,[+] Dr. M. R. Jones
School of Biochemistry
University of Bristol
Biomedical Sciences Building
University Walk
Bristol BS8 1TD, UK

Y. K. Ngeow
Department of Biological Sciences
National University of Singapore
14 Science Drive 4, Singapore 117543, Singapore

DOI: 10.1002/adma.201704073

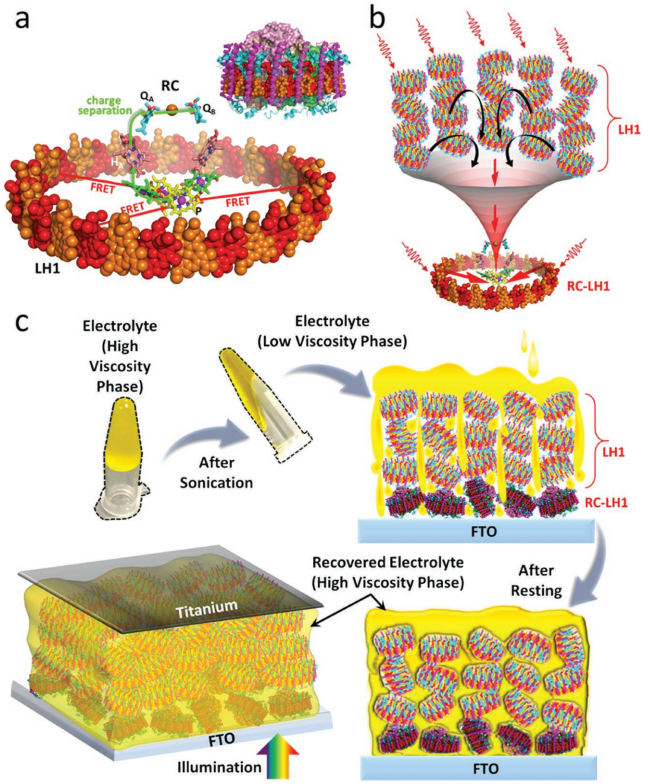

Figure 1. Properties and fabrication of photobioelectrochemical cells. a) The *Rba. sphaeroides* RC–LH1 complex (inset) comprises a central RC (solid object) surrounded by a cylindrical LH1 protein (ribbons). Energy absorbed by the LH1 bacteriochlorophylls (ring of alternating red and orange spheres) and carotenoids (not shown) flows by resonance transfer (red arrows) to the P bacteriochlorophyll pair of the RC (sticks, yellow carbons), initiating charge separation (green arrows) to H_A (sticks, pink carbons), Q_A, and Q_B (sticks, cyan carbons) (see Figure S1 and Section 3 of the Supporting Information for more details). b) In natural photosystems, light energy harvested by an extended antenna pigment-protein system is concentrated by directional energy transfer onto a smaller number of photovoltaic reaction center pigment proteins, where energy is trapped through charge separation. In the present study, this is mimicked in 3D by coating a base layer of RC–LH1 proteins with multilayers of LH1 antenna proteins (not drawn to scale). This demonstrates the possibility of expansive collection of photons by extended layers of light-harvesting antennae that concentrate the excitonic energy to a smaller number of energy traps, which is analogous to the mechanism of a satellite dish that collects weak signals from a wide space and concentrates them on a sensor at a focal point. c) To achieve device fabrication, the gel-phase succinonitrile/T_2/T^- electrolyte was liquefied by sonication and applied to one or more protein multilayers that had been spin coated on the working electrode (see Video S1 in the Supporting Information for a demonstration of the gel–liquid–gel transition at room temperature). During the subsequent resting period, the electrolyte soaked into the protein coating after which the counter electrode was placed on the gel surface and the cell sealed with epoxy resin. Individual complexes are expected to be oriented randomly throughout the protein film. Spin coating can be used to lay down complex architectures, such as that illustrated where a base coating of RC–LH1 complexes (bottom layer) is overlaid with upper coatings of LH1 complexes (three upper layers).

a significantly lower, steady-state output.[13,16,17,19–21,23–25] Proposals that this decline is due to limitations imposed by slow mediator diffusion[17,27,28] have been corroborated by measurements with a rotating disk working electrode to provide mixing.[19] Effective electrical connection of these proteins to both the working and counter electrodes often requires the assembly of mediator-accessible protein monolayers at the surface of the working electrode, resulting in relatively low absorption of actinic light. Photocurrent densities achieved with RC and RC–LH1 complexes have typically occupied the range from a few nA cm^{-2} to several tens of μA cm^{-2} with, as discussed below, a couple of reports of higher currents.[19,29]

Progression from liquid- to solid-state device architectures could create new opportunities for enhancement of photocurrent output and elimination of photocurrent decline due to diffusional limitations. However, interfacing proteins with suitable conductive materials presents considerable challenges as this often requires one or more coating steps involving elevated temperatures or high-velocity deposition. As an example, three thermal evaporation steps were used to deposit electron acceptor materials on the protein layer in the only solid-state RC photobioelectrochemical device described to date.[29] Given the sensitivity of pigment proteins to thermal or mechanical stress, it is important to develop fabrication processes for interfacing conductive materials with proteins under nondenaturing conditions. Similar concerns affect a wider range of synthetic light-harvesting materials that exhibit sensitivity to stress conditions such as elevated temperature. Furthermore, the use of protein multilayers to achieve high absorbance raises the question of how proteins in different layers can be electrically connected to both electrodes. One approach to increasing absorbance is to use nanostructured electrode materials in combination with a diffusible mediator[19,30] or entrapment in a redox hydrogel,[31] but such nanostructuring to achieve an increased electrode surface area adds complexity to cell fabrication procedures.

In this work, we manufactured a range of new solid-state photobioelectrochemical cells based on multilayers of an engineered variant of the *Rhodobacter* (*Rba.*) *sphaeroides* RC–LH1 complex or its component LH1 and RC pigment proteins (see Section 3 of the Supporting Information). Employing a similar RC–LH1 complex, a photocurrent of ≈160 μA cm^{-2} was recently obtained when the protein was drop-casted onto a nanostructured rough-silver electrode in a three-electrode liquid cell employing a rotating disk electrode.[19] This was comparable to a photocurrent density of ≈120 μA cm^{-2} achieved by an RC solid state device exposed to extremely strong (10 W cm^{-2}) monochromatic excitation.[29] The photobioelectrochemical cells described here were designed with a view to improve the steady-state photocurrent output achievable under standard illumination conditions by eliminating limitations imposed by slow mediator diffusion, while also enhancing light absorption through a multilayer architecture that can be fabricated under entirely benign conditions using planar electrode materials and simple deposition procedures.

Our new design for a solid-state, two electrode RC–LH1 cells combined, for the first time, a gel-state interface between electrodes, a permeating disulfide-thiolate (T_2/T^-) electron carrier and spin-coated multilayers of protein (see the Experimental Section in the Supporting Information). A variety of cell architectures were explored to address the question of whether, in a man-made 3D photosystem, light-harvesting and charge-separating functions work best when combined in all layers in the device or when confined to separate layers. Investigation of the latter included placing separately purified LH1 and RC

proteins in different layers to mimic natural 2D photosystems in which specialized light-harvesting proteins (the antenna) pass harvested excited state energy to a smaller number of photovoltaic RC proteins (the transducers) through directional energy transfer (Figure 1b). We also used "fast-recombining" RC and RC–LH1 complexes that, due to a single amino acid change (AM260W), assemble without a ubiquinone at the Q_A electron acceptor site in the RC[32] (Figure S1, Supporting Information). In AM260W RCs, the recombination lifetime of the final product of charge separation ($P^+H_A^-$, ≈17 ns[33]) is eight orders of magnitude shorter than that in the native RC ($P^+Q_B^-$, ≈1–2 s), but the absorbance spectrum and gross structure of the RC or RC–LH1 complex are not affected.

Proteins in the multilayers were connected to the electrodes using a conductive interface based on succinonitrile ($N{\equiv}C{-}CH_2{-}CH_2{-}C{\equiv}N$), a highly polar organic plastic crystalline material that, due to lattice defects and rotational vacancies, can provide a nonconducting matrix for a conducting salt.[34] This matrix was suffused by an equimolar mixture of the *N*-tetramethylammonium ($^+NMe_4$) salt of 5-mercapto-1-methyltetrazole (T^-) and di-5-(1-methyltetrazole) disulfide (T_2),[35,36] producing a plastic gel-phase material with a high ionic and molecular diffusivity.[37] While gels are typically liquefied by heating, crucially for work with labile pigment proteins, we have discovered that this material undergoes a reversible gel-to-liquid transition under mechanical vibration. As sonication did not produce significant heating of the succinonitrile/electrolyte mix, this provided a means of permeating layers of photoactive protein with the electrolyte matrix at room temperature (Figure 1c).

Prepared salts of the T_2/T^- redox couple (**Figure 2**a) were used as an equimolar mixture and had a vacuum potential of –4.8 eV (Figure S2, Supporting Information). Both $^+NMe_4$ T^- and T_2 were dissolved in molten succinonitrile at a concentration of 0.2, 0.4, 0.6, or 0.8 M (Figure 2b). The gels formed on cooling exhibited a mechano-induced transition to liquid phase that reversed on resting (Video S1, Supporting Information). Concentrations of $^+NMe_4$ T^- and T_2 of 0.8 M represented an upper limit beyond which the succinonitrile mix did not form a gel. The viscosities of the gels were measured by rheometry (Anton Paar MCR 702 TwinDrive) at a low shear rate of 0.005 s^{-1} for 30 s, producing a plateau with a slight slope (Figure 2c). The 0.2 M electrolyte produced a gel state with the highest viscosity, higher T_2/T^- concentrations producing progressively lower viscosities. After 30 s, gels were sheared at an increasing rate that confirmed non-Newtonian shear thinning behavior with final liquid viscosities in the mPa s range (Figure 2c, right). Charge flux through the electrolytes was measured by electrochemical impedance spectroscopy, the decreasing diameter of the semicircles in the resulting Nyquist plots (Figure 2d) indicating an enhancement of ion flux and charge transfer to the counter electrode as the concentrations of T_2 and T^- were increased. An electrolyte concentration of 0.8 M was selected for the fabrication of most devices to maximize charge transfer while retaining a gel phase when dissolved in succinonitrile.

The first set of working electrodes was fabricated by depositing multilayers of RC–LH1 protein onto a conductive fluorine-doped tin oxide (FTO) glass substrate through up to 20 cycles of spin coating and partial drying (**Figure 3**a). Achieving an optimal

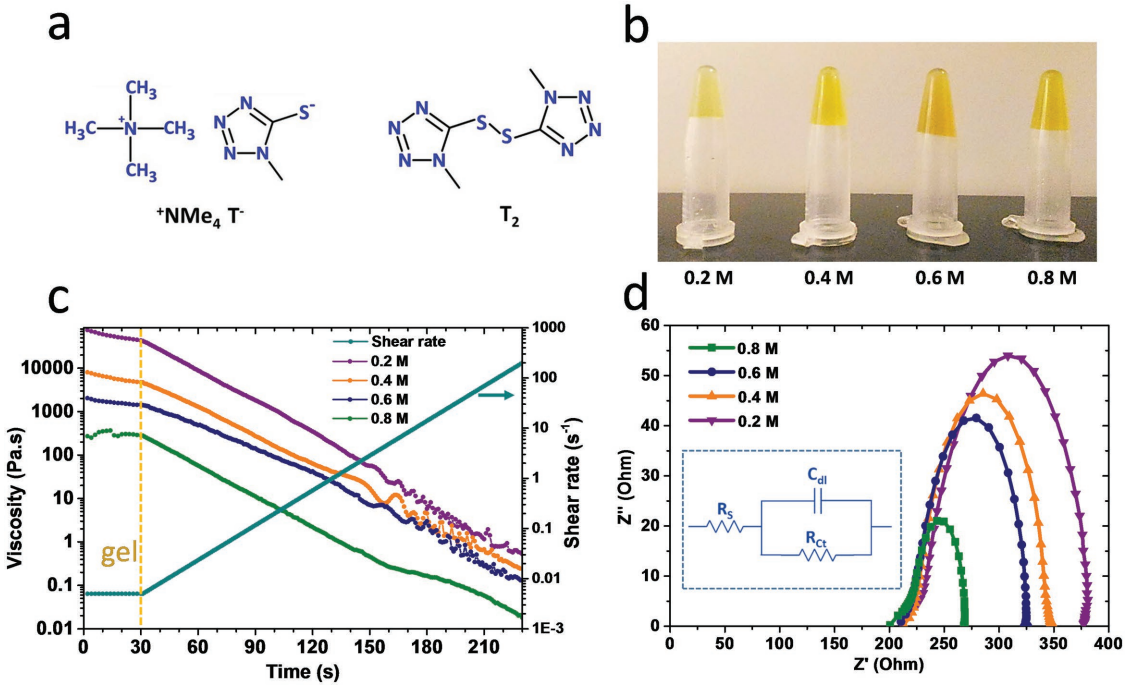

Figure 2. Characterization of the gel electrolyte. a) The electrolyte was an equimolar mixture of $^+NMe_4$ T^- and T_2 in succinonitrile. b) Images of gel phase electrolytes formed from increasing equimolar mixtures of $^+NMe_4$ $T^-$and T_2. Concentrations above 0.8 M were not used as this resulted in a liquid electrolyte rather than the desired gel. c) Change in viscosity on increased shear rate for different concentrations of electrolyte. The 0.2, 0.4, 0.6, and 0.8 M electrolytes had viscosities of ≈75, ≈8, ≈2, and ≈0.3 kPa s, respectively, in the gel form. d) Nyquist plots for dummy cells comprising different concentrations of electrolyte between two Ti electrodes. Inset: Equivalent circuit model for the Nyquist plot. R_s, C_{dl}, and R_{ct} denote series resistance, double layer capacitance, and charge transfer resistance, respectively.

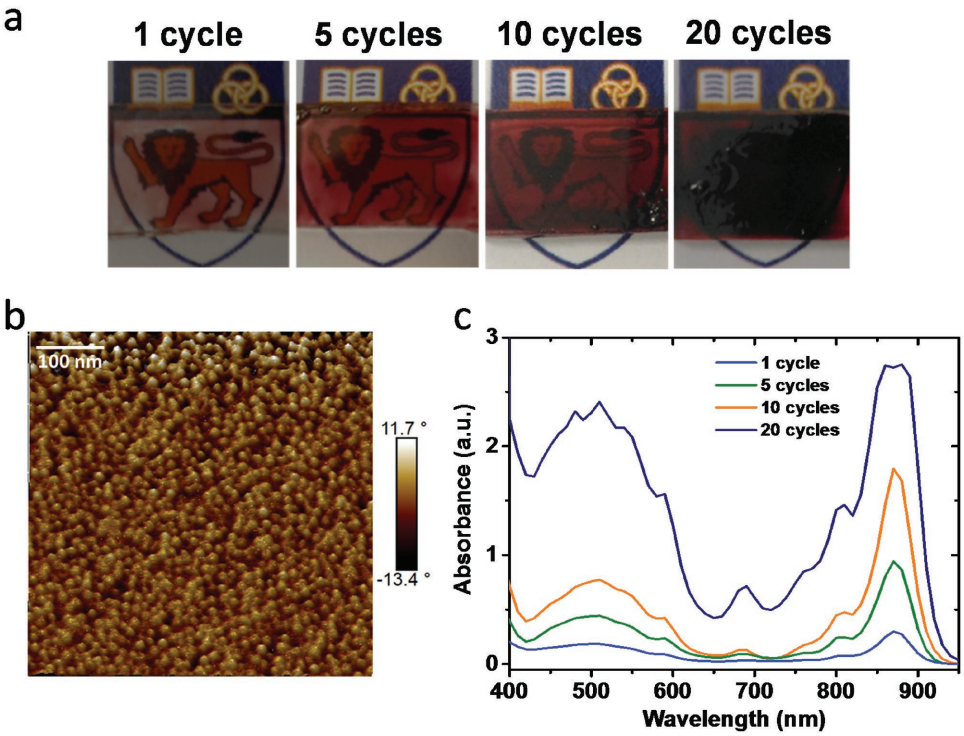

Figure 3. Deposition of the protein layer. a) Images of RC–LH1 films on FTO-glass prepared by one or more cycles of spin-coating, taken against a colored background. b) AFM phase image of the surface of an RC–LH1 multilayer film formed by a single cycle of spin coating. c) Absorbance spectra of RC–LH1 films. The detector became saturated for the thickest films producing spectral distortion that was also contributed to by light scatter.

coverage of protein on the 1 cm^2 substrate required use of a protein stock solution at a concentration of around 150×10^{-6} M (600 absorbance units at 875 nm); at this concentration, the protein solution (in a 20×10^{-3} M Tris (pH 8.0)/0.04% *n*-dodecyl *β*-D-maltopyranoside buffer) was very viscous but could still be pipetted. The most consistent coverage was achieved with a two-stage spin cycle and a 4-min period of partial drying between coats (see the Experimental Section in the Supporting Information), and it was possible to deposit up to 20 coats before adding further layers became impracticable. The use of spin-coating freed-up selection of the material for the working electrode, as no functionalization or direct binding interactions were needed to attach proteins. In addition, as described below, it enabled the controlled deposition of successive multilayers made up from different proteins. Atomic force microscopy (AFM) of an RC–LH1 multilayer deposited by a single cycle of spin coating revealed an upper surface comprising particles with dimensions and spacings consistent with closely packed RC–LH1 complexes (Figure 3b; see Figure S3 in the Supporting Information for a sample topogram). The lack of a regular topology from one particle to another suggested a random orientation of individual proteins within the film. Absorbance spectra showed that the amount of protein adhering after the first coating was greater than after subsequent coatings (Figure 3c). Beyond 10 cycles, the measured absorbance spectrum became distorted due to the thickness of the protein multilayer and contributions from light scattering (Figure 3c).

Profilometry showed that the thickness of the deposited protein multilayer increased from ≈4 μm for a single coating to ≈45 μm for 20 coatings (Figure S4, Supporting Information). Assuming that an individual RC–LH1 complex in its detergent micelle has a mean diameter of around 15 nm, consistent with the particle separation in the image in Figure 3b and atomic-level structural information on RC–LH1 complexes, these thicknesses would be consistent with multilayers comprising 267 and 3000 protein molecules, respectively. The thickness of protein film deposited by spin coating showed very good reproducibility (Figures S4 and S5, Supporting Information), enabling comparisons across multiple cells and investigation of the relative merits of equivalent loadings of RC–LH1 and LH1 proteins as light-harvesting materials. Importantly, the absorbance spectra of deposited proteins did not vary significantly in line shape from that in solution, demonstrating that the pigment proteins had not been damaged by spin-coating and subsequent treatments.

Cells for photochronoamperometry were constructed by drop casting 10 μL of sonicated, liquid-phase electrolyte onto a protein-coated FTO-glass electrode (Figure 1c). After allowing the liquid electrolyte to spread across the entire protein area and soak into the protein coating, the Ti-coated back electrode was brought into contact with the electrolyte layer and the cell was sealed with epoxy resin. This resulted in only a very thin layer of gel phase electrolyte connecting the protein multilayer to the counter electrode, the aim being to facilitate a high ion flux and current density.

Photochronoamperometry revealed that the photocurrent density in response to one sun illumination increased as the concentrations of T_2/T^- increased in cells fabricated with a single coating of RC–LH1 complexes (**Figure 4**a). All subsequent experiments were therefore performed with 0.8 M electrolyte, which had the lowest viscosity and highest charge flux (Figure 2d). The photocurrent density increased as the amount of deposited RC–LH1 protein increased (Figure 4b), up to an average of

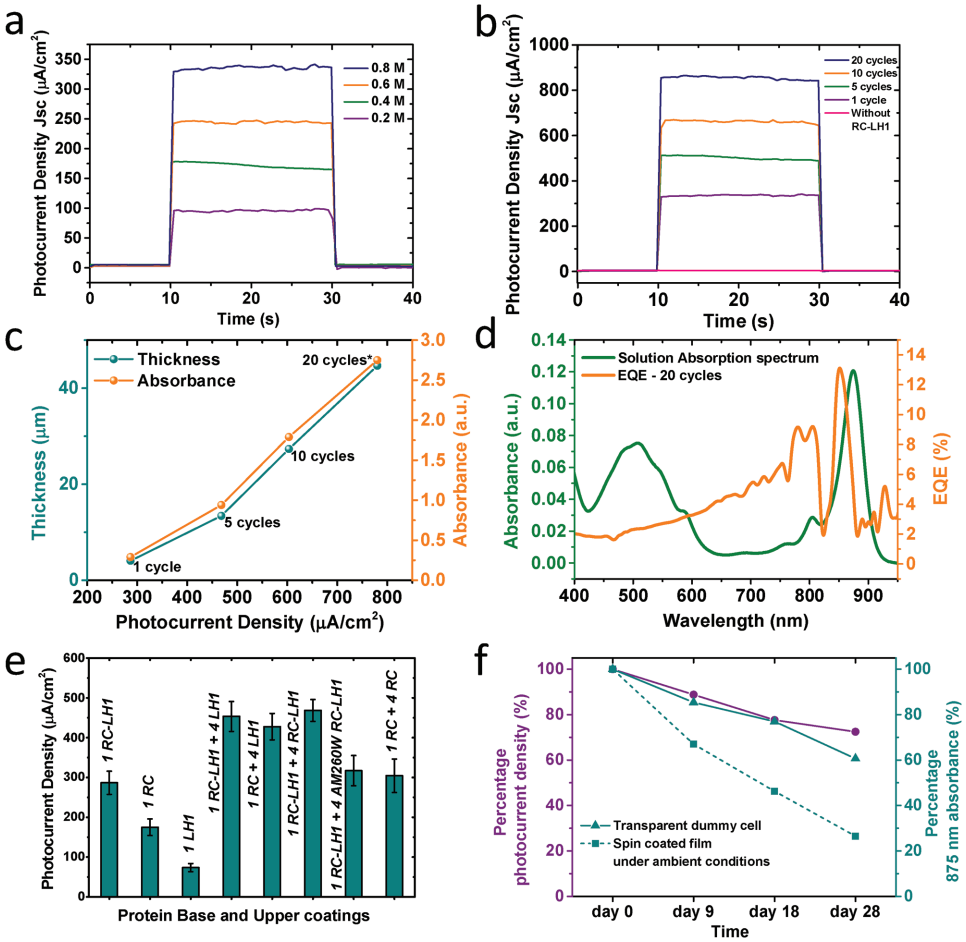

Figure 4. Photocurrents and stability of photobioelectrochemical cells. a) Photocurrent density over 20 s illumination as a function of electrolyte concentration for an RC–LH1 multilayer formed by a single cycle of spin coating. b) Photocurrent density over 20 s illumination as a function of multiple cycles of spin coating for RC–LH1 complexes with 0.8 M electrolyte. c) Variation of photocurrent density with the thickness and absorbance at 875 nm of the RC–LH1 multilayer; *the absorbance value corresponding to 20 cycles of spin coating is a slight underestimate as the spectrophotometer detector reached saturation. d) EQE action spectrum for a 20 cycle RC–LH1 cell compared to the absorbance spectrum of RC–LH1 complexes in solution; both exhibit bands specific to (mainly) LH1 at 875 nm and the RC at 805 nm. e) Photocurrent densities for different protein base and upper coatings, with 0.8 M electrolyte. f) Protein and photocurrent stability over 28 d at ambient illumination and temperature.

780 μA cm^{-2} for an electrode fabricated by 20 cycles of spin coating; the highest output achieved with an individual cell of this type was 860 μA cm^{-2} (Figure 4b). Cells yielded only a negligible photocurrent of 0.5 μA cm^{-2} without the protein coating (Figure 4b), demonstrating that the RC–LH1 complexes were the source of the substantial photocurrent. With greater than one cycle of spin coating, the photocurrent density was linearly proportional to the measured thickness of the RC–LH1 multilayer (Figure 4c).

An action spectrum of external quantum efficiency (EQE) versus excitation wavelength for an RC–LH1 cell formed from 20 cycles of spin coating was compared to the solution RC–LH1 spectrum (Figure 4d). A peak EQE of ≈13% was observed attributable to the characteristic LH1 absorbance. In the near-infrared, the absorbance spectrum principally comprises a prominent band centered at 875 nm attributable to 16 LH1 bacteriochlorophylls and two RC bacteriochlorophylls and a lower band at 805 nm attributable to two RC bacteriochlorophylls. In the action spectrum, the relative contribution of the (mainly) LH1-specific band was strongly reduced relative to the shorter wavelength RC-specific band. This underrepresentation of LH1 to an action spectrum of photocurrent generation has been seen previously[13] and interpreted as showing that the photocurrent output is limited by electron transfer in the cell rather than light harvesting by LH1 (see Section 4 in the Supporting Information for a discussion). Action spectra recorded for RC–LH1 cell fabricated by a single cycle of spin coating also showed this phenomenon (Figure S6, Supporting Information), confirming that it was not due to self-shading by LH1 pigments in the thicker protein multilayers.

Regarding the mechanism of photocurrent generation, the observed anodic photocurrent implied that photoexcitation of the pigment-protein coating produced electron donation to the FTO-glass working electrode from a sufficiently reducing excited or anion state (**Figure 5**, cyan and blue arrows), with rereduction by the Ti counter electrode of the resulting oxidized pigment(s), most probably P^+ (Figure 5, gold). As the vacuum potential of T_2/T^- (Figure 5, yellow) was much deeper than that of FTO-glass or Ti, we conclude that the T_2/T^- facilitated

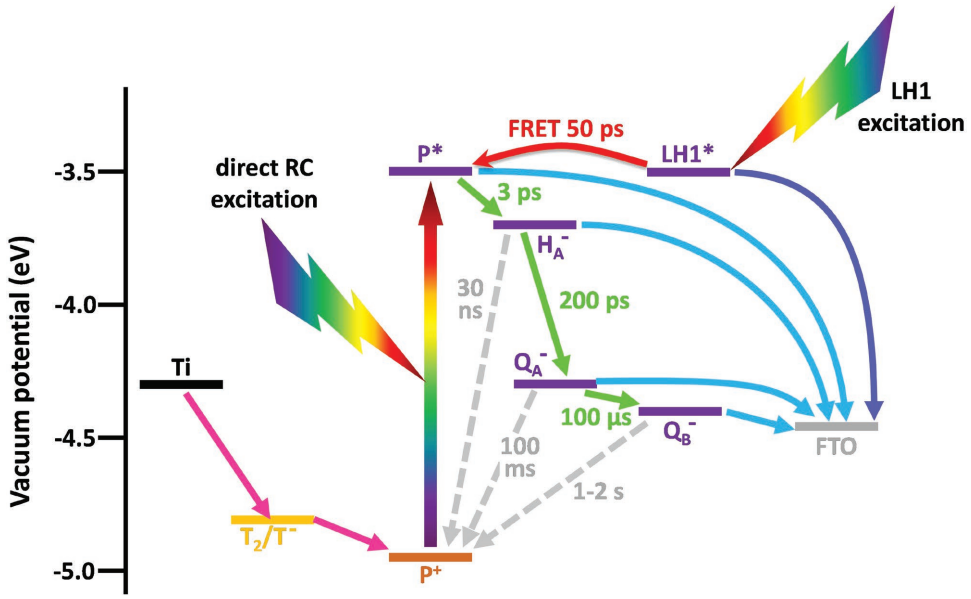

Figure 5. Mechanism of photocurrent generation in cells with an FTO-glass working electrode. Vacuum potentials of reducing and oxidizing components of the RC are shown in purple and brown, respectively. Direct excitation of the RC, or excitation of LH1 pigments followed by Förster resonance energy transfer (FRET) to the RC (magenta arrow), triggers charge separation by promoting a pair of bacteriochlorophyll cofactors in the RC (P) into their first singlet excited state (P* – rainbow arrow). Charge separation (green arrows) proceeds through the radical pairs $P^+H_A^-$, $P^+Q_A^-$, and $P^+Q_B^-$ (see Figure 1a for the spatial arrangement of these cofactors and Section 3 of the Supporting Information for a more detailed description). At each stage, rapid forward electron transfer (green arrows) outcompetes slow radical pair recombination (gray dashed arrows). The mechanism of multistep charge separation and associated lifetimes for separation and recombination events has been reviewed.[8,10,11] Reduction of P^+ mediated by the electrolyte (red arrows) would isolate a long-lived anion state, most probably Q_B^- in wild-type RCs and H_A^- in fast-recombining AM260W RCs. The cyan and blue arrows indicate possible processes for reduction of the working electrode by RCs or LH1 complexes, respectively, some or all of which can operate depending on which protein complex makes up the base coating of the device.

electron transfer from the counter electrode to the photooxidized species in the protein coating (Figure 5, magenta arrows). One expectation is that the ease of penetration of the 0.8 M electrolyte should be greater than that of lower concentrations as its liquid-state viscosity is the closest to that of water at room temperature (Figure 2c), and this may have contributed to the higher current seen with 0.8 M T_2/T^- compared to other concentrations.

Given the similarity in vacuum potential of FTO-glass and Ti (Figure 5), a prediction is that cells of a reverse electrode configuration should be functional. This was the case, a photocurrent of −270 µA cm^{-2} being obtained when RC–LH1 complexes were spin coated onto a Ti back electrode (single round) and FTO-glass was used as the counter electrode (Figure S7, Supporting Information). This was almost identical, but with reverse polarity, to the average of 287 µA cm^{-2} obtained for an equivalent cell with a single coating of RC–LH1 complexes on FTO-glass.

The modular nature of the *Rba. sphaeroides* photosystem was exploited to investigate the mechanism of charge injection into the working electrode, by comparing the average current from a single coating of purified RCs, or a single coating of purified LH1 light-harvesting pigment proteins, with the 287 µA cm^{-2} obtained from a single coating of the combined RC–LH1 complex. An average current of 74 µA cm^{-2} was obtained with LH1 (Figure 4e), demonstrating that some charge injection can happen directly through an LH1 excited state (LH1*) acting as a sensitizer (Figure 5, blue arrow), as this protein does not itself carry out charge separation. The mechanism would be equivalent to that proposed to operate in TiO_2-based solar cells employing light-harvesting proteins as the photosensitizer.[38–40] A strongly oxidising LH1 cation will result that can be rereduced, in the present case, by the permeating T_2/T^- electrolyte.

Cells with a single coating of purified RCs gave an average current of 175 µA cm^{-2} (Figure 4e). This demonstrated that electron injection must also be able to occur from an RC excited or anion state (Figure 5, cyan arrows). As the lowest-energy RC excited state (P*) has a lifetime of only 3–5 ps, it seems more likely that this state was one or more of the multiple anions produced, sequentially, during charge separation within the RC (Figure 5, green arrows). The identity of this anion was explored further using fast-recombining RCs, as discussed in Section 5 of the Supporting Information.

Although either RCs or LH1 proteins could individually drive a photocurrent, the strongest output was obtained using the combined RC–LH1 complex. Data from more strongly pigmented, multicoating cells showed that although LH1 and RC–LH1 complexes have similar absorbance spectra, the latter was still much more effective at generating a photocurrent. Cells fabricated with either one or ten coatings of LH1 produced currents of 74 and 114 µA cm^{-2}, respectively, while cells fabricated with either one or ten coatings of RC–LH1 produced currents of 287 and 603 µA cm^{-2}, respectively (Table S1, Supporting Information). This was despite similar in light-harvesting capacities, as judged by the intensity of the LH1 absorbance band at 875 nm.

The mechanism of photocurrent generation by multilayers of photosynthetic protein is a little explored and poorly

understood area, but is likely to involve energy transfer between protein layers. To clarify how different layers supported photocurrent generation in multilayer cells, four coatings of LH1 complexes were deposited over a single base coating of either RC–LH1 or RC complexes. Average photocurrents were 453 and 428 μA cm^{-2}, respectively (Figure 4e; Table S1, Supporting Information), much higher than the 287/175 μA cm^{-2} that could be obtained with just a single base coating of RC–LH1 or RC complexes. This strongly suggested that the additional LH1 coatings play a light-harvesting function, passing excited state energy to the base coating to power electrode reduction.

These current enhancements supported the proposal that the photochemical process that produced the current was electron injection into the working FTO–glass electrode from the adjacent base coating of protein, followed by reduction of the photooxidised protein by the permeating T_2/T^- electrolyte. The alternative mechanism, reduction of photoexcited bacteriochlorophylls at the protein–electrolyte interface, would be expected to produce strongly reducing LH1 bacteriochlorophyll anions. It is unlikely that subsequent migration of electrons through multilayers of LH1 protein to the working electrode would be efficient in the absence of suitable mediators.

An interesting finding was that the average current of 468 μA cm^{-2} obtained by overlaying a single base coating of RC–LH1 complexes with four further RC–LH1 coatings was almost identical to the 453 μA cm^{-2} achieved using four additional coatings of LH1 protein (Figure 4e). The implication is that having additional charge-separating RCs in the upper coatings did not waste harvested energy. This was intriguing, as a feature of natural photosystems that supports their high quantum efficiencies is that unproductive charge separation is avoided in the extensive light-harvesting regions of the photosystem, being limited to a small number of specialist RC proteins where charge separation is electrically connected to an external proton-motive electron transfer chain to achieve energy conservation.

Two possible explanations could be put forward for this apparent lack of energy wastage. The first, which seems unlikely, is that the rate of LH1 → LH1 energy transfer between adjacent RC–LH1 complexes in the upper coatings of the cell is much faster than the rate of LH1 → RC energy transfer (trapping) within individual RC–LH1 complexes (lifetime of around 50 ps), and so wasteful charge separation in the upper coatings is not competitive with productive energy migration through hundreds or thousands of LH1 antenna proteins. The second is that charge separation takes place in the upper layers but is not wasteful, instead making a positive contribution to the photocurrent through the creation of metastable radical pairs throughout the bulk of the device, such that any decrease in light-harvesting efficiency due to trapping is compensated for.

To investigate this point further, cells were fabricated in which a base coating of RC–LH1 complexes was overlaid with four coatings of fast-recombining AM260W RC–LH1 complexes. The resulting average photocurrent was 317 μA cm^{-2}, substantially lower than the 468 μA cm^{-2} obtained with four additional coatings of normal RC–LH1 or the 453 μA cm^{-2} obtained with four additional coatings of LH1 protein (Figure 4e). We attribute this to the ≈17 ns charge-separated state formed in the AM260W RCs being less effective in supporting charge conduction through the bulk of the protein multilayer than the 10^8 longer-lived charge-separated state formed in the native RC.

We also examined the impact of charge separation taking place throughout the bulk of a protein multilayer by fabricating cells with either one or five coatings of RCs. Average currents were 175 and 304 μA cm^{-2}, respectively (Figure 4e). As RCs have evolved to trap excitation energy through highly efficient ultrafast charge separation, it is likely that the current enhancement on adding more RCs was due to charge separation in the upper coatings and RC to RC electron transfer, rather than a light-harvesting effect involving inter-RC energy transfer. As discussed in Section 6 of the Supporting Information, experiments with multilayer cells fabricated from fast-recombining AM260W RCs supported this interpretation. Reducing the lifetime of the longest-lived RC radical pair by eight orders of magnitude substantially reduced the photocurrents that were produced from RC multilayers.

Finally, in addition to enabling very stable photocurrent densities during short periods continuous illumination (Figure 4a,b), studies with sealed and dummy cells suggested that the long-term stability of the RC–LH1 complex was enhanced by embedding it in the succinonitrile/T_2/T^- gel. A dummy transparent RC–LH1/T_2/T^- cell employing two FTO-glass electrodes showed 39% drop in absorbance at 875 nm over 28 d of storage at room temperature and a continuous ambient illumination of ≈2 W m^{-2}, indicating slow degradation of the LH1 pigment protein (Figure 4f; Figure S8a, Supporting Information). In good agreement with this, the photocurrent obtained from an equivalent cell with a Ti counter electrode showed a 27% decrease in current density (Figure 4f). For a spin coated RC–LH1 film on FTO-glass not incorporated into a cell with electrolyte, the 875 nm absorbance dropped by 73% over the same period (Figure 4f; Figure S8b, Supporting Information), suggesting a protective effect of the gel electrolyte.

In conclusion, the protein-based photobioelectrochemical cells described above combined a number of innovations in cell design, fabrication and materials that produced a maximum fivefold improvement in photocurrent amplitude compared to the highest previously reported current from a comparable device.[19] Our previous research with this particular RC–LH1 complex in liquid state photoelectrochemical cells with diffusible electrolytes produced steady-state photocurrents ranging between 0.15 and 8 μA cm^{-2} [23,24,41,42] and we attribute the maximally two orders of magnitude increase in current density seen in the present work to a combination of the dense protein multilayers achievable with spin coating and the charge conduction enabled by a high concentration of permeating gel phase electrolyte. Spin coating also facilitated controlled deposition on unfunctionalised electrodes of multiple multilayers of different types of photosynthetic protein, making possible exploration of photocurrent mechanism and evaluation of strategies for maximizing output. The architecture of some devices followed natural principles in which a limited number of photovoltaic centers are fed with excited-state energy by a larger light-harvesting system, but we also revealed that metastable charge separation throughout all layers can bring about current enhancements. The succinonitrile/T_2/T^- electrolyte material removes commonly observed diffusive restrictions on the steady-state photocurrent density and, due to its vibration-induced phase transition, could be combined with

labile biological materials in a simple way without inducing protein damage. In broader terms, this methodology could provide a means of interfacing an ionic electrolyte with any photoactive species that cannot tolerate exposure to the harsh conditions often required for device fabrication.

Supporting Information

Supporting Information is available from the Wiley Online Library or from the author.

Acknowledgements

D.J.K.S and M.R.J acknowledge support from the Biotechnology and Biological Sciences Research Council of the UK (project BB/I022570/1). S.K.R. and S.C.T. acknowledge the financial support from MOE AcRF 1 (R-284-000-134-112 and R-284-000-129-133), and acknowledge Janice Tan and Sue Li Chan of Anton Paar Singapore Pte. Ltd for their support on the rheological measurements.

Conflict of Interest

The authors declare no conflict of interest.

Keywords

bio-photovoltaics, mechanoresponsive gels, photosynthetic reaction centers, solid-state solar cells

Received: July 21, 2017
Revised: September 12, 2017
Published online: December 18, 2017

[1] R. Croce, H. van Amerongen, *Nat. Chem. Biol.* **2014**, *10*, 492.
[2] G. D. Scholes, G. R. Fleming, A. Olaya-Castro, R. van Grondelle, *Nat. Chem.* **2011**, *3*, 763.
[3] X. Xie, G. A. Crespo, G. Mistlberger, E. Bakker, *Nat. Chem.* **2014**, *6*, 202.
[4] O. Yehezkeli, R. Tel-Vered, J. Wasserman, A. Trifonov, D. Michaeli, R. Nechushtai, I. Willner, *Nat. Commun.* **2012**, *3*, 742.
[5] S. K. Ravi, S. C. Tan, *Energy Environ. Sci.* **2015**, *8*, 2551.
[6] A. Efrati, C.-H. Lu, D. Michaeli, R. Nechushtai, S. Alsaoub, W. Schuhmann, I. Willner, *Nat. Energy* **2016**, *1*, 15021.
[7] K. Schrantz, P. P. Wyss, J. Ihssen, R. Toth, D. K. Bora, E. A. Vitol, E. A. Rozhkova, U. Pieles, L. Thöny-Meyer, A. Braun, *Catal. Today* **2017**, *284*, 44.
[8] G. Feher, J. P. Allen, M. Okamura, D. Rees. *Nature* **1989**, *339*, 111.
[9] S. Niwa, L.-J. Yu, K. Takeda, Y. Hirano, T. Kawakami, Z.-Y. Wang-Otomo, K. Miki, *Nature* **2014**, *508*, 228.
[10] W. Zinth, J. Wachtveitl, *Chemphyschem* **2005**, *6*, 871.
[11] M. R. Jones, *Biochem. Soc. Trans.* **2009**, *37*, 400.
[12] M.-H. Ham, J. H. Choi, A. A. Boghossian, E. S. Jeng, R. A. Graff, D. A. Heller, A. C. Chang, A. Mattis, T. H. Bayburt, Y. V. Grinkova, A. S. Zeiger, K. J. Van Vliet, E. K. Hobbie, S. G. Sligar, C. A. Wraight, M. S. Strano, *Nat. Chem.* **2010**, *2*, 929.
[13] M.-J. den Hollander, J. G. Magis, P. Fuchsenberger, T. J. Aartsma, M. R. Jones, R. N. Frese, *Langmuir* **2011**, *27*, 10282.
[14] A. Sumino, T. Dewa, N. Sasaki, M. Kondo, M. Nango, *J. Phys. Chem. Lett.* **2013**, *4*, 1087.
[15] D. J. K. Swainsbury, V. M. Friebe, R. N. Frese, M. R. Jones, *Biosens. Bioelectron.* **2014**, *58*, 172.
[16] H. Yaghoubi, Z. Li, D. Jun, E. Lafalce, X. Jiang, R. Schlaf, J. T. Beatty, A. Takshi, *J. Phys. Chem. C* **2014**, *118*, 23509.
[17] R. Caterino, R. Csiki, A. Lyuleeva, J. Pfisterer, M. Wiesinger, S. D. Janssens, K. Haenen, A. Cattani-Scholz, M. Stutzmann, J. A. Garrido, *ACS Appl. Mater. Interfaces* **2015**, *7*, 8099.
[18] J. Gebert, C. Reiner-Rozman, C. Steininger, V. Nedelkovski, C. Nowak, C. A. Wraight, R. L. C. Naumann, *J. Phys. Chem. C* **2015**, *119*, 890.
[19] V. M. Friebe, J. D. Delgado, D. J. K. Swainsbury, J. M. Gruber, A. Chanaewa, R. van Grondelle, E. von Hauff, D. Millo, M. R. Jones, R. N. Frese, *Adv. Funct. Mater.* **2016**, *26*, 285.
[20] S. M. Mirvakili, J. E. Slota, A. R. Usgaocar, A. Mahmoudzadeh, D. Jun, M. N. Mirvakili, J. T. Beatty, J. D. W. Madden, *Adv. Funct. Mater.* **2014**, *24*, 4789.
[21] H. Yaghoubi, E. Lafalce, D. Jun, X. Jiang, J. T. Beatty, A. Takshi. *Biomacromolecules* **2015**, *16*, 1112.
[22] M. Kondo, K. Iida, T. Dewa, H. Tanaka, T. Ogawa, S. Nagashima, K. V. P. Nagashima, K. Shimada, H. Hashimoto, A. T. Gardiner, R. J. Cogdell, M. Nango, *Biomacromolecules* **2012**, *13*, 432.
[23] S. C. Tan, L. I. Crouch, M. R. Jones, M. Welland, *Angew. Chem., Int. Ed.* **2012**, *51*, 6667.
[24] S. C. Tan, L. I. Crouch, S. Mahajan, M. R. Jones, M. E. Welland. *ACS Nano* **2012**, *6*, 9103.
[25] S. C. Tan, F. Yan, L. I. Crouch, J. Robertson, M. R. Jones, M. E. Welland. *Adv. Funct. Mater.* **2013**, *23*, 5556.
[26] M. Chatzipetrou, F. Milano, L. Giotta, D. Chirizzi, M. Trotta, M. Massaouti, M. R. Guascito, I. Zergioti. *Electrochem. Commun.* **2016**, *64*, 46.
[27] E. Katz, *J. Electroanal. Chem.* **1994**, *365*, 157.
[28] A. Takshi, J. D. Madden, J. T. Beatty. *Electrochim. Acta* **2009**, *54*, 3806.
[29] R. Das, P. J. Kiley, M. Segal, J. Norville, A. A. Yu, L. Wang, S. A. Trammell, L. E. Reddick, R. Kumar, F. Stellacci, N. Lebedev, J. Schnur, B.D. Bruce, S. Zhang, M. Baldo, *Nano Lett.* **2004**, *4*, 1079.
[30] H. Yaghoubi, M. Schaefer, S. Yaghoubi, D. Jun, R. Schlaf, J. T. Beatty, A. Takshi, *Nanotechnology* **2017**, *28*, 054006.
[31] K. P. Sokol, D. Mersch, V. Hartmann, J. Z. Zhang, M. Nowaczyk, M. Rögner, A. Ruff, W. Schuhmann, N. Plumeré, E. Reisner, *Energy Environ. Sci.* **2016**, *9*, 3698.
[32] J. P. Ridge, M. E. van Brederode, M. G. Goodwin, R. van Grondelle, M. R. Jones. *Photosynth. Res.* **1999**, *59*, 9.
[33] K. Gibasiewicz, M. Pajzderska, J. A. Potter, P. K. Fyfe, A. Dobek, K. Brettel, M. R. Jones, *J. Phys. Chem. B* **2011**, *115*, 13037.
[34] P.-J. Alarco, Y. Abu-Lebdeh, A. Abouimrane, M. Armand, *Nat. Mater.* **2004**, *3*, 476.
[35] M. Wang, N. Chamberland, L. Breau, J.-E. Moser, R. Humphry-Baker, B. Marsan, S. M. Zakeeruddin, M. Grätzel, *Nat. Chem.* **2010**, *2*, 385.
[36] X. Xu, K. Cao, D. Huang, Y. Shen, M. Wang. *J. Phys. Chem. C* **2012**, *116*, 25233.
[37] D. Hwang, D. Y. Kim, S. M. Jo, V. Armel, D. R. MacFarlane, D. Kim, S.-Y. Jang, *Sci. Rep.* **2013**, *3*, 3520.
[38] Q. Fu, C. Zhao, S. Yang, J. Wu, *Mater. Lett.* **2014**, *129*, 195.
[39] D. Yu, M. Wang, G. Zhu, B. Ge, S. Liu, F. Huang, *Sci. Rep.* **2015**, *5*, 9375.
[40] M. Nagata, M. Amano, T. Joke, K. Fujii, A. Okuda, M. Kondo, S. Ishigure, T. Dewa, K. Iida, F. Secundo, Y. Amao, H. Hashimoto, M. Nango, *ACS Macro Lett.* **2012**, *1*, 296.
[41] S. K. Ravi, Z. Yu, D. J. K. Swainsbury, J. Ouyang, M. R. Jones, S. C. Tan. *Adv. Energy Mater.* **2017**, *7*, 1601821.
[42] V. K. Singh, S. K. Ravi, J. W. Ho, J. K. C. Wong, M. R. Jones, S. C. Tan, *Adv. Funct. Mater.* **2017**, 1703689, https://doi.org/10.1002/adfm.201703689.